Journal of Heat and Mass Transfer Research

Journal homepage: http://jhmtr.semnan.ac.ir

Semnan University

Three-Dimensional Viscous Dissipative Flow of Nanofluids Over a Riga Plate

Pachiyappan Ragupathi[a], Abdul Kafoor Abdul Hakeem[*,a], Bhose Ganga[b], Sohail Nadeem[c,d]

[a]*Department of Mathematics, SRMV College of Arts and Science, Coimbatore-641020, India.*
[b]*Department of Mathematics, Providence College for Women, Coonoor-643104, India.*
[c]*Mathematics and its Applications in Life Sciences Research Group, Ton Duc Thang University, Ho Chi Minh City, Vietnam.*
[d]*Faculty Mathematics and Statistics, Ton Duc Thang University, Ho Chi Minh City, Vietnam.*

PAPER INFO

Paper history:
Received: 2020-08-22
Revised: 2020-12-02
Accepted: 2020-12-02

Keywords:
Viscous Dissipation;
Riga plate;
Three-dimensional flow;
Nanofluids;
Runge-Kutta 4th order method;
Shooting Method.

ABSTRACT

In this study, the physical perspectives on three-dimensional flow of $H_2O/NaC_6H_9O_7$ base fluids with Fe_3O_4/Al_2O_3 nanoparticles are comparatively investigated under the effect of viscous dissipation using Runge-Kutta 4th order numerical procedure. With the help of similarities transformations, the mathematical model which are described as partial differential equations are transmuted into ordinary differential equations. As said, the Runge-Kutta method, assisted by the shooting strategy, is designed to deal numerically with the resulting set of non-linear differential equations. Highlights of the flow-field and thermal field are illustrated quantitatively in plots. Results for local skin friction coefficients and local Nusselt number are reported and analyzed tabularly. The accuracy of present study is verified in comparison to existing literatures and we have identified an astounding understanding. Also, results indicate that, the velocity profile is enhanced by the modified Hartmann number and stretching ratio parameters. The $H_2O - Al_2O_3$ nanofluid, in fact, has elevated skin friction values and is also more suitable for increasing the rate of heat transfer.

DOI: 10.22075/jhmtr.2020.21120.1300

1. Introduction

In various industrial and technical fields like MHD generators, liquid cooling blankets for reactors fusion, flow meters, oil technologies and pumps, etc., fluid flow under magnetohydrodynamics (MHD) plays a key role. The electromagnetic body forces, which control the movement of fluid molecules in the boundary layer, can also affect electrically conducting fluencies. The use of external magnetic field (~1 Tesla) affects fluids with high electrical conductivity. A standard MHD flow monitor is used with such a mechanism. For weak conducting fluid the induced current generated by an external magnetic field is not sufficient. A wall-parallel Lorentz strength for higher and more efficient flow control is therefore needed for an outside electric field.

Due to a wide range of possible uses in the biological, optical and computer sectors, nanoparticle science is increasingly an area of considerable scientific interest. Due to tremendous applications in chemistry, food and industrial applications, shipping, electronics, biomedicine, nuclear rectors, vehicles, drug distribution and biological sensors, nanotechnology has gained considerable attention in recent years. There are several reports on nanofluids in various geometries. Turkyilmazoglu [1] considered the single phase nanofluids in fluid mechanics and analysed their hydrodynamic linear stability. A numerical study for the buoyancy effects on nanofluid flow past a convectively heated vertical Riga-plate was done by Ahmad et al. [2]. Gholinia et al. [3] examined the nanoparticle shape and thermal ray on a $CuO/C_2H_6O_2 - H_2O$ hybrid base nanofluid inside a porous enclosure using Darcy's law numerically. Similar investigations on nanofluids can be found from the most recent papers of Turkyilmazoglu [4], Gholinia et al. [5], Ghadikolaei and Gholinia [6], Dibaei and Kargarsharifabad [7], Tajik et al. [8] and Gholinia et al. [9].

[*]*Corresponding Author: Abdul Kafoor Abdul Hakeem ,Department of Mathematics, SRMV College of Arts and Science, Coimbatore-641020, India.*
Email: abdulhakeem6@gmail.com

Gailities [10] firstly introduced an equipment called an electromagnetic actuator (Riga plate) which includes electromagnetic actuators and static magnets, alternatively placed in a smooth area. Such arrangements have produced a Lorentz wall parallel force, which quickly decreases in the normal range to the surface. The Riga plate can be used for decreasing pressure drags and skin friction in submersible warships by preventing the breakdown of the boundary layer as a helpful agent. The properties of nanofluid flow induced by Riga plates were not very examined by analysts. Hakeem et al. [11] observed on the effect on the Carreau nanofluid flow through an electromagnetic plate through a poreful medium of exponentially variable viscosity and permeability. The non-darcian three dimensional flow of nanoparticulates Fe_3O_4/Al_2O_3 with $H_2O/NaC_6H_9O_7$ base fluids past a platform of Riga embedded within a poreful medium was further examined by Ragupathi et al. [12]. The uniform heat-source / sink effect on a Fe_3O_4/Al_2O_3 3D flow of nanoparticles with different base fluids past a Riga-platform was numerically observed by Ragupathi et al. [13]. The three-dimensional non-linear radiative flow of nanfluid over a Riga plate was considered by Hakeem et al. [14]. A velocity slip and radiation impact were inspected on the stagnation points flow and heat transfer past the permeable stretching / shrinking Riga plate by Nasir et al. [15]. Shafiq et al. [16] recently recorded the effect of radiation on Walters' B fluid stagnating point flow to a Riga plate. The effect on mixed convective flow to the Riga platform consisting of the micropolar TiO_2 −kerosene / water nanoparticles was investigated by Zaib et al. [17]. Abbas et al. [18] spoke about promoting and opposing the mixed convection Casson nanofluid flow through a porous Riga platform with chemical reactions.ion Casson nanofluid flow through a porous Riga platform with chemical reactions.

The result of internal heat generation and thermal deposition on viscous dissipating viscoplastic fluid transmission through the Riga plate were considered in Iqbal et al. [19]. Nayak et al. [20] investigated the effects on radiative $NaCl/CNP$ nanofluid flow past a convectively heated vertical Riga plate by homogenous-heterogeneous reactions. Anjum et al. [21] inspected the stagnating point flow to the variable thick Riga platform of thermal stratification and slip conditions. The transient rotational flow of the radiative nanofluids over the Riga platform with variable properties was explored by Shaw et al. [22].

The distinctive nature of fluids is defined as Newtonian or non-Newtonian, based on their viscosity behavior as a function of shear rate, stress, deformation rate etc. Newtonian fluids remain a continuous viscosity irrespective of how quickly they are forced to flow through a pipe or channel. Non-Newtonian fluids are strikingly different from Newtonian fluids, meaning that either a non-linear relationship between shear pressure and shear rate has a yield stress or viscosity that is dependent on time or deformation rate. Actually, most of the fluids are non-newtonian, so their viscosity depends on the rate of shear.

Such studies on rheological fluids are arousing for their enhancing importance in the science and engineering. In any case, a not many non-Newtonian liquid flow issues in fluid mechanics got consideration, as a result of their novel test to physicists, engineers and mathematicians. As a part of this many researchers, Hussain et al. [23], Hakeem et al. [24], Rundora et al. [25], Bayareh et al. [26], Saranya et al. [27] and Eid and Mahny [28] contributed their work. Also, the Casson model, designed specifically to inspect these non-Newtonian fluids has attracted many researchers. For instance, Durgaprasad et al. [29], Raju et al. [30], Zaigham Zia et al. [31] and Prashu [32] have discussed their recent researches on Casson model.

Viscous dissipation often works as a heating element and creates potential medium temperatures. This is also the rate at which the movement of the liquid in viscous fluid by porous means is converted into heat per unit volume. In extreme gravitational fields as e.g., on large planets, space with large amounts of gas and in geological procedures in internal fluids to assorted frames, the significant effects of viscous dissipation may also occur. Many proceedings have been speculated engaging the effects of viscous dissipation in heat transfer. The numerical simulation for the heating effects like viscous and Joule in 3D MHD flow with thermal and mass fluxes were considered for the Muhammad et al. [33]. Kumar et al. [34] reported Joule heating characteristics and viscous dissipation of Oldroyd B's thermal nanofluid flow. The optimum study of nanomaterial radiated flow with viscous dissipation and thermal source was performed by Saleem et al. [35]. Nayak et al. [36] investigated into Boungiorno model for partial slip and viscous dissipating effects on the hyperbolic radiation flow of nanofluid through an internal heat-induced vertical permeable Riga plate. Mahanthesh and Gireesha [37] discussed scrutinizing the thermal radiation, viscous dissipation and Joule heating effects of the fluid-particle suspension with Casson fluid in convective two-phase Marangoni flow. Research on the impact of viscous dissipation on nanofluid flow under different geometries has recently been produced by Upreti et al. [38], Hussanan et al. [39], Ramandevi et al. [40], and some interesting applications are given in Ghaffarpasand [41],Hassanzadeh and Nasrollahzadeh [42], Noghrehabadi et al. [43].

Motivated from the above literature in this study we analyze the viscous dissipation effect on the three-dimensional boundary layer nanofluid flow over a Riga plate using nanoparticles Fe_3O_4 and Al_2O_3 on base liquids. The novelty of the present study is highlighted below.

- This investigation focuses on comparing the viscous dissipation properties between the combination of nanofluids.

Two types of base fluids and nanoparticles are selected (H_2O+Fe_3O_4,H_2O+Al_2O_3,$NaC_6H_9O_7$+$Fe_3O_4$$NaC_6H_9O_7$+ Al_2O_3). The non-Newtonian behaviour of $NaC_6H_9O_7$ base fluid is discussed by employing Casson model.

- The Grinberg term [10] has been used to model the electro MHD flow of nanofluids.
- Numerical solutions are carried out by fourth order Runge-Kutta method with shooting iteration technique.
- Outcomes in the absenteeism of nanoparticles when matched with Wang [44], Hayat et al. [45] and Ganesh Kumar et al. [46] remained in noble agreement.

2. Mathematical Formulation

All We consider a laminar, steady, three-dimensional, incompressible based nanofluids flow over a Riga plate. Fe_3O_4 and Al_2O_3 are chosen to be the nanoparticles. The flow is caused by the Riga plate which is put in a position $z = 0$. The $xy-$plane bares the plate where z equals zero $(z = 0)$ and the domain where $z > 0$ is chosen to assume that the flow occurs as it can be seen in Figure 1. Let the $x-$direction stretching velocity be $u = U_w(x) = ax$ and the $y-$direction stretching velocity is $v = V_w(y) =$ byof the Riga plate, respectively. Further, attention is paid towards the viscous dissipation effects without neglecting it. In addition, the thermal balance of the base fluids and nanoparticles are assumed true. We also presume, that the rheological state can be written (see Abbas et al. [18] for more details) for an incompressible Casson fluid as.

$$\tau = \tau_0 + \mu\gamma^* \tag{1}$$

Or

$$\tau_{i_j} = \begin{cases} 2\left(\dfrac{\sqrt{2\prod}\mu_B + p_y}{\sqrt{2\prod}}\right) eij\ .\ \Pi_c < \Pi \\ 2\left(\dfrac{\sqrt{2\prod_C}\mu_B + p_y}{\sqrt{2\prod_C}}\right) eij.\ \Pi_c > \Pi \end{cases} \tag{2}$$

The above assumption takes the form of the following controlling equations of continuity; momentum and energy (see Ganesh Kumar et al. [46]).

$$\frac{\partial u}{\partial x} + \frac{\partial v}{\partial y} + \frac{\partial w}{\partial z} = 0 \tag{3}$$

$$u\frac{\partial u}{\partial x} + v\frac{\partial u}{\partial y} + w\frac{\partial u}{\partial z} = \nu_{nf}\left(1 + \frac{1}{\beta}\right)\frac{\partial^2 u}{\partial z^2} + \frac{\pi\, j_0 M_0}{8\rho_{nf}}\ e^{\left(\frac{-\pi z}{a_1}\right)} \tag{4}$$

$$u\frac{\partial v}{\partial x} + v\frac{\partial v}{\partial y} + w\frac{\partial v}{\partial z} = \nu_{nf}\left(1 + \frac{1}{\beta}\right)\frac{\partial^2 v}{\partial z^2} \tag{5}$$

$$u\frac{\partial T}{\partial x} + v\frac{\partial T}{\partial y} + w\frac{\partial T}{\partial z} = \alpha_{nf}\frac{\partial^2 T}{\partial z^2} + \frac{\mu_{nf}}{(\rho C_p)_{nf}}\left(\left(\frac{\partial u}{\partial z}\right)^2 + \left(\frac{\partial v}{\partial z}\right)^2\right) \tag{6}$$

The conditions at the boundary are:

$$\begin{cases} u = U_w(x)\,.\,v = Vw(x). \\ w = 0\,.\ T = T_w\ \ at\ z = 0 \\ u \to 0\,.\ v \to 0\,.\ T \to T_\infty\ \ as\ \ z \to \infty \end{cases} \tag{7}$$

where the fluid temperature of the wall is T_w.

$$\begin{cases} u = axf'(\eta)\ \ .\ \ v = ayg'(\eta)\ . \\ w = -\sqrt{av_f}\big(f(\eta) + g(\eta)\big)\ . \\ \theta(\eta) = \dfrac{T - T_\infty}{T_w - T_\infty}\ \ .\ \ \eta = z\sqrt{\dfrac{a}{\nu_f}} \end{cases} \tag{8}$$

3. Similarity transformation and non-dimensionalization

The continuity equation Eq. (3) is automatically satisfied by assisting the similarity transformations in Eq. (8) whereas the transformations change the Eqs. (4), (5) and (6) as

$$(\beta^{-1}(1+\beta))\,S_1 f''' + (f+g)f'' - f'^2 + QS_2\, e^{-\eta A} = 0 \tag{9}$$

$$(\beta^{-1}(1+\beta))\,S_1 g''' + (f+g)g'' - g'^2 = 0 \tag{10}$$

$$\left(\frac{S_4}{S_3}\right)\left(\frac{1}{Pr}\right)\theta'' + (f+g)\,\theta' + \left(\frac{S_3}{S_4}\right)\left(\frac{1}{S_5}\right)Ec\,(f''^2 + g''^2) = 0 \tag{11}$$

The transformed boundary conditions are

$$\begin{cases} f = 0\ \ .\ \ g = 0\ \ .\ \ f' = 1\ \ . \\ g' = \alpha\ \ .\ \ \theta = 1\ \ at\ \ \eta = 0 \\ f' \to 0\ \ .\ \ g' \to 0\ \ .\ \ \theta \to 0\ \ as\ \ \eta \to \infty \end{cases} \tag{12}$$

Here the primes denote differentiation with respect to η and

$$S_1 = \frac{1}{(1-\phi)^{2.5}\left(1 - \phi + \phi\left(\frac{\rho_s}{\rho_f}\right)\right)}$$

$$S_2 = \frac{1}{\left(1-\phi+\phi\left(\frac{\rho_s}{\rho_f}\right)\right)}$$

$$S_3 = \left(1-\phi+\phi\left(\frac{(\rho C_p)_s}{(\rho C_p)_f}\right)\right)$$

$$S_4 = \frac{k_{nf}}{k_f}.$$

$$S_5 = (1-\phi)^{2.5}\left(1-\phi+\phi\left(\frac{(\rho C_p)_s}{(\rho C_p)_f}\right)\right)$$

Also, Pr $= \frac{\mu_f (C_p)_f}{k_f}$ is the Prandtl number, $Q = \frac{\pi j_0 M_0 x}{8\rho_f U_w^2}$ is the modified Hartmann number, $A = \frac{\pi}{a_1}\left(\frac{a}{\nu}\right)^{-1/2}$ is the dimensionless parameter and $Ec = \frac{{U_w}^2}{(C_p)_f (T_w - T_\infty)}$ is the Eckert number.

4. Physical Quantities of Interest

In this study, the quantities of practical interest are the local skin friction coefficients C_{fx} . C_{fy} and the local Nusselt number Nu_x defined as follows

$$C_{fx} = \frac{\tau_w x}{\rho_f U_w^2} \quad . \quad C_{fx} = \frac{\tau_w y}{\rho_f U_w^2}$$
$$. \; Nu_x = \frac{x q_w}{k_f (T_w - T_\infty)} \tag{13}$$

where τ_{wx} and τ_{wy} is the surface shear stresses along the $x-$ and $y-$directions and q_w is the heat flux, and are given by

$$\begin{cases} Re_x^{1/2} C_{fx} = (1-\phi)^{-2.5}\left(1+\frac{1}{\beta}\right) f''(0) \\ Re_x^{1/2} C_{fy} = \alpha^{-3/2}(1-\phi)^{-2.5}\left(1+\frac{1}{\beta}\right) g''(0) \\ Re_x^{-1/2}\, Nu_x = -S_4\, \theta'(0) \end{cases} \tag{14}$$

5. Numerical method for solution

Equations (9)-(11) are highly non-linear and it is very tough to find solutions to them analytically. So, an alternate way is to assist the numerical methods. Here we opt to use Runge-Kutta method, a classical method. In order to assist this method we first need to transform the BVP(boundary value problem) into an IVP(initial value problem), this is done with shooting technique. The transformed IVP is

$$y_1' = y_2$$
$$y_2' = y_3$$
$$y_3' = \frac{-(y_1+y_4)\, y_5 - Q\, S_2\, e^{-\eta A} + {y_2}^2}{S_1\left(1+\frac{1}{\beta}\right)} \tag{15}$$
$$y_4' = y_5$$
$$y_5' = y_6$$
$$y_6' = \frac{-(y_1+y_4)\, y_6 + {y_5}^2}{S_1\left(1+\frac{1}{\beta}\right)} \tag{16}$$
$$y_7' = y_8$$
$$y_8' = -\left(\frac{S_3}{S_4}\right) Pr\,(y_1+y_4)\, y_8 + \left(\frac{1}{S_5}\right) Ec\, Pr\,({y_3}^2 + {y_6}^2) \tag{17}$$

And the conditions at the boundary are

$$\begin{cases} y_1(0) = 0 \;.\; y_4(0) = 0 \;.\; y_2(0) = 0 \;. \\ y_5(0) = \alpha \quad and \quad y_7(0) = 1 \end{cases} \tag{18}$$

The initial guesstimate was supplied to $y_3(0)$ i.e., $f''(0)$, $y_6(0)$ i.e., $g''(0)$ and $y_8(0)$ i.e., $\theta'(0)$. Then the results are checked with the boundary conditions and the convergence criterion, if it is satisfied no further modification in the guess values is required. If not the guess values are again modified until it matches the boundary conditions (18) and the convergence criterion of 10^{-8}.

6. Results and Discussion

A fourth order RK approach with shooting techniques acquires the numerical problem analysis. The graphic representation supports the analysis of the parameters related to this problem. We'll switch to the Newtonian base fluid (H_2O) case, assuming $\beta \to \infty$ Table 1 lists the thermophysical properties of the basic fluids and their nanoparticles and the corresponding nanofluid models in Table 2. Comparing the works of Wang [44], Hayat et al. [45] and Ganesh Kumar et al. [46], the precision of the numerical plan was achieved. The validity of the current findings is interpreted in accordance with Table 3.

Figures 2(a) and 2(b) indicate the velocity distribution lead expressed by dimensionless parameter A. Noteworthy is the velocity appropriation for broad estimates of dimensionless parameter A reduces. This result is due to a decrease in the thickness of the momentum boundary layer. Therefore, Al_2O_3 nanoparticles have an over-powering effect with base fluids than Fe_3O_4 nanoparticles on their velocity acquisition.

Figure 3(a) shows velocity appropriation with α for H_2O based nanoparticles. From this figure, it is seen that a development in α prompts to diminish the velocity appropriation along x−direction while a backwards propensity can be seen for velocity appropriation along y−direction. The rising estimations of $\alpha = b/a$ start an addition in b or rundown in a. In this manner, alongside

the y −direction the speed increments also, downturns along x −direction. Practically this is identical with the case of $NaC_6H_9O_7$ based nanoparticles as could be seen in Figure 3(b).

Various Hartmann number Q shifts are seen in the estimates for velocity appropriation with Figures 4(a) and 4(b). The higher Q results in velocity and boundary layer grade amplification. So that higher Q calculations are based on the strength of the external load of electricity which is distributed over the normal level and heads up to Lorentz power. Speed appropriation increases in this way. In this manner, velocity appropriation improves.

Figure 5 is planned to show the essential features of Casson parameter β on the x − and y −direction velocities. The Casson parameter in the tie-up between the viscosity and yield stress of the fluid, so an elevation in β leads to upsurge the fluid viscosity level. Thus it results in a thinner momentum boundary layer and lower fluid velocity.

Figures 6(a) and 6(b) unveil the characteristics of stretching ratio parameter α on the temperature distribution. The intensity of heat present near the plate comparatively equals the heat present in the ambient region with the rising values of α. This response is due to the expansion of thermal boundary region.

The Eckert number usually refers to the comparison of the Kinetic energy to nanofluid enthalpy and is often used to describe the magnitude of fluid self-heating. This provoke a temperature profile shift, as shown in Figures 7(a) and 7(b). As Eckert number values are increased the kinetic energy involved helps for the increment of temperature profile.

Survey of literature proves that the signiface of nanofluid as expending because of their upgraded thermal conductivity, which is a result of the suspension of nanoparticles, whose warm conductivity is substantially higher than the base fluids. Clearly higher estimation of ϕ helps advancing the temperature of the nanofluid. These adjustments in the temperature profile are recorded in Figure 8(a) for water based nanofluid and Figure 8(b) for $NaC_6H_9O_7$ based nanofluid. This figure make evident that, in the entire province the temperature profile is stirred with the advantage of ϕ.

The pattern of modified Hartmann Q on the friction coefficient is interpreted by Figures 9(a) and 9(b). It is stated that shear stress improves in the x −direction when Hartmann number is adjusted to higher. The Lorentz force with its inherent nature of resistivity and its velocity decreasing quality is explained by the presence of the magnetic field, by which shear stress take over the responsibility of regulating the flow dynamics. The slow down of the fluid velocity in the reaction enhances the co-efficient of the skin friction.

In Figures 10(a) and 10(b), the local skin friction decreases in x −direction by increasing the stretching ratio values α. This behavior is explained by the exercise of viscous drag force on the flow field which corresponds to a decrease and increase in the thickness of the boundary momentum layer and in the skin friction factor. However, Figures 11(a) and 11(b) indicates a contrast existence in y-direction.

At large flow rates, the fluidic system's temperature regulation is controlled not just by the temperature gradients in the system, but also by the implications of dissipation due to the fluid's inner friction. With the increase of the Eckert number, the amount of Nusselt number lessens as the thermal limit layer just next to a plate is thinner as is seen in Figures 12(a) and 12(b).

The effect of the related parameters on the friction factor for both base fluids is shown in separate tables Table 4 and Table 5. We noted that we have increased local skin friction coefficient for Q and β. Furthermore, Table 6 displays the numerical value of α and Q for local Nusselt number.

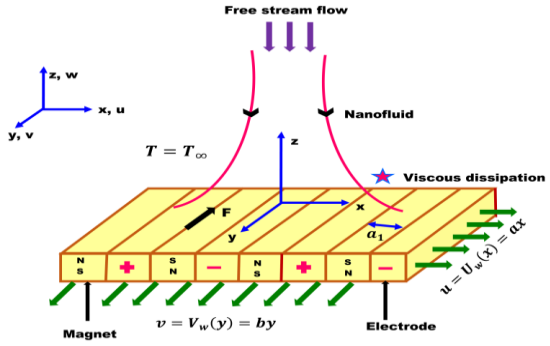

Figure 1. Physical Configuration

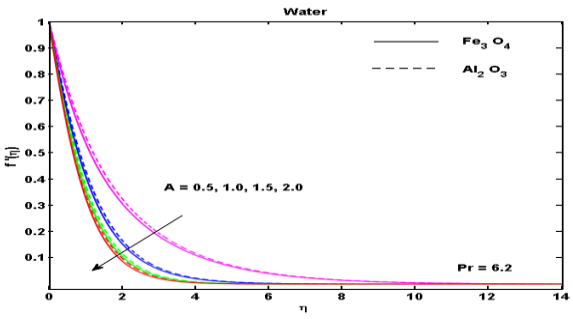

(a)

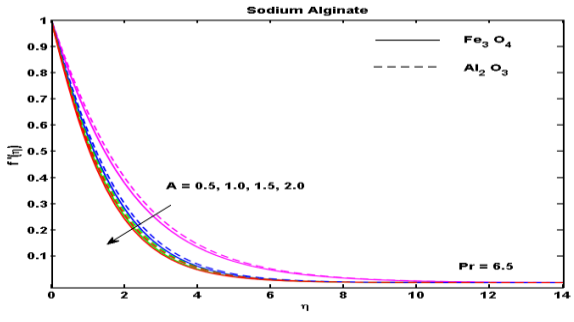

(b)

Figure 2. Curves of A on f′(η)for Q = 0.1 . α = 0.6 . ϕ = 0.1 . β = 0.5.

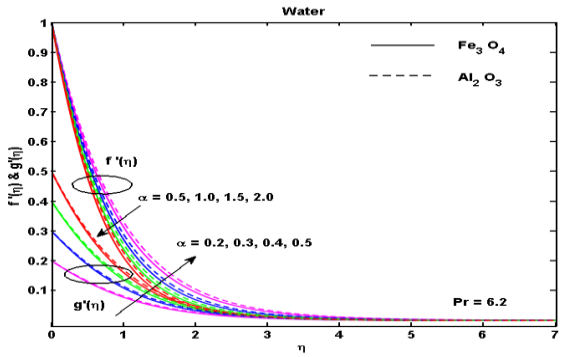

(a)

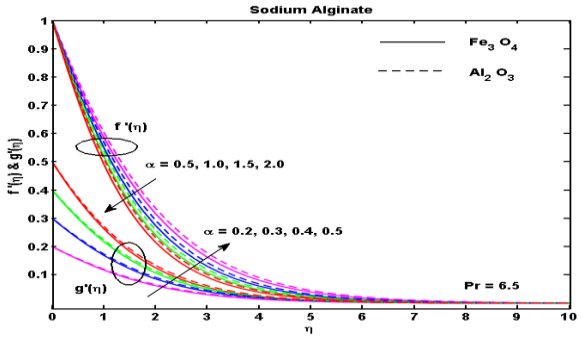

(b)

Figure 3. Curves of α on $f'(\eta)$and $g'(\eta)$ for $Q = 0.1$. $A = 0.8$. $\phi = 0.1$. $\beta = 0.5$

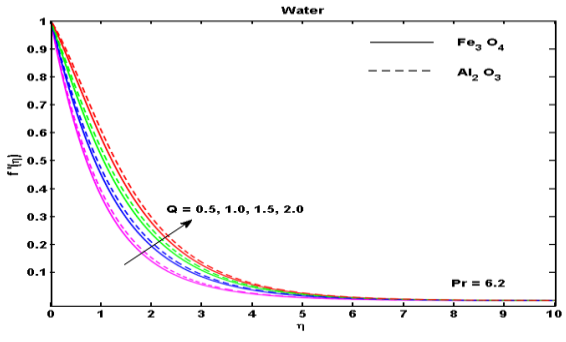

(a)

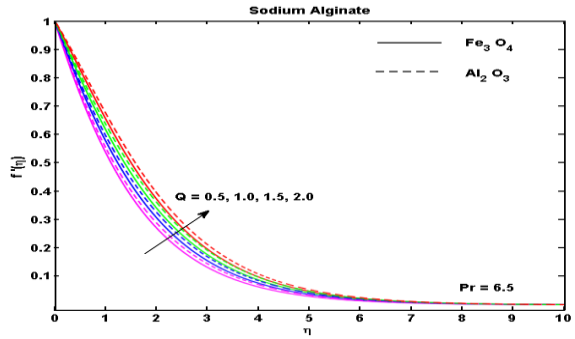

(b)

Figure 4. Curves of Q on $f'(\eta)$ for $A = 0.8$. $\alpha = 0.6$. $\phi = 0.1$. $\beta = 0.5$

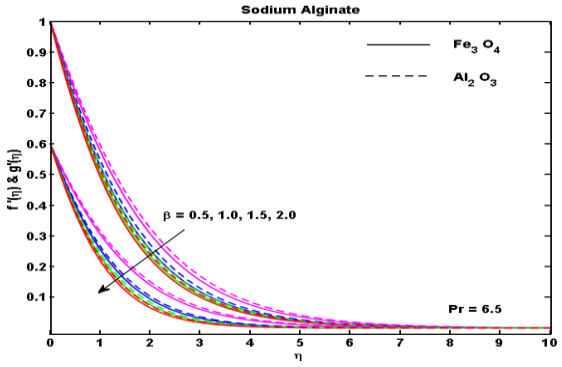

Figure 5. Curves of β on $f'(\eta)$and $g'(\eta)$ for $Q = 0.1$. $A = 0.8$. $\phi = 0.1$. $\alpha = 0.6$.

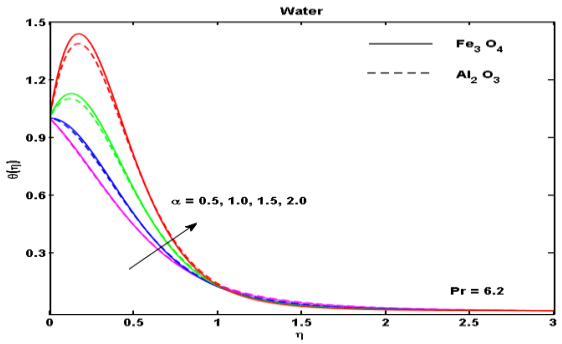

(a)

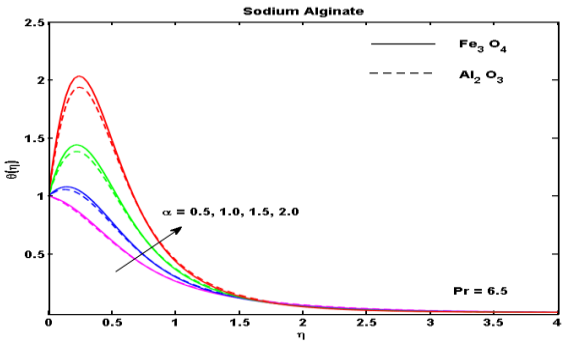

(b)

Figure 6. Curves of α on $\theta(\eta)$ for $Q = 0.1$. $A = 0.8$. $\phi = 0.1$. $\beta = 0.5$. $Ec = 0.5$.

Table 1. Base fluid and nanoparticle properties [27].

	Water	**Sodium Alginate**	Fe_3O_4	Al_2O_3
ρ $(Kg\ m^{-3})$	997	989	5180	3970
C_p $(J\ Kg^{-1}\ K^{-1})$	4179	4175	670	765
k $(W\ m^{-1}\ K^{-1})$	0.613	0.6376	9.7	40
ν_f $(m^2\ s^{-1})$	8.90x 10^{-4}	-	-	-
Pr	6.2	6.5	-	-

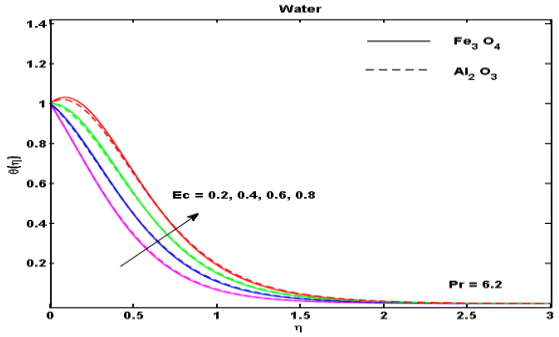

(a)

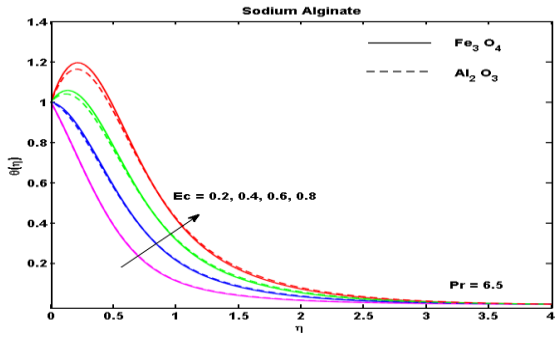

(b)

Figure 7. Curves of Ec on $\theta(\eta)$ for $Q = 0.1$. $A = 0.8$. $\phi = 0.1$. $\alpha = 0.6$. $\beta = 0.5$.

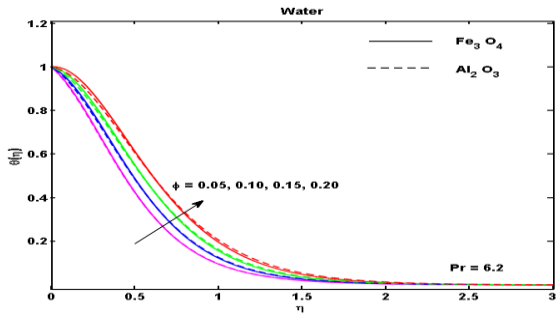

(a)

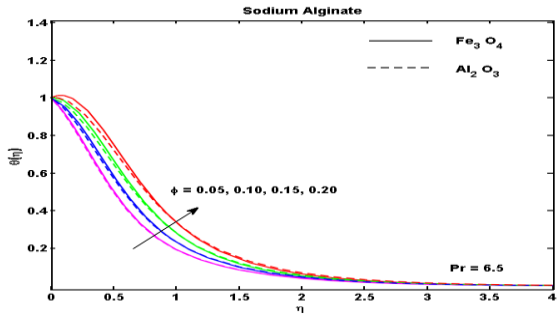

(b)

Figure 8. Curves of ϕ on $\theta(\eta)$ for $Q = 0.1$. $A = 0.8$. $\alpha = 0.6$. $\beta = 0.5$. $Ec = 0.5$.

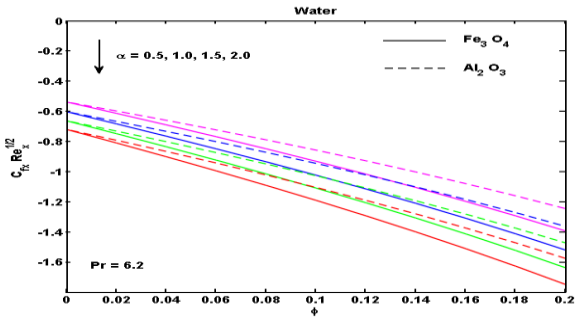

(a)

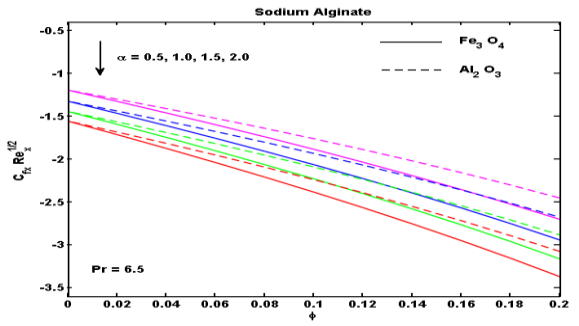

(b)

Figure 9. Curves of α on the local skin friction coefficient in the x −direction for $Q = 0.1$. $A = 0.8$. $\phi = 0.1$. $\beta = 0.5$.

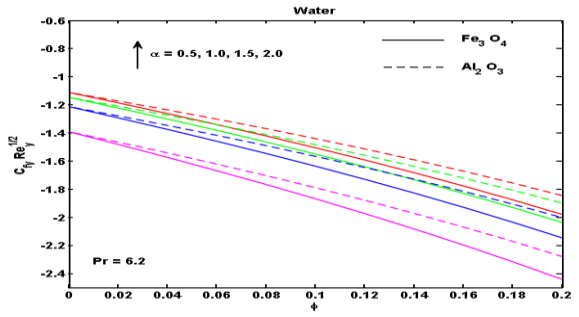

(a)

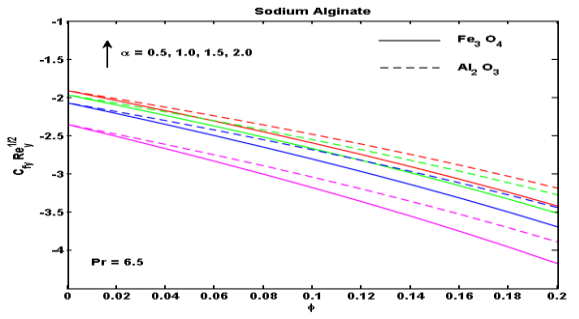

(b)

Figure 10. Curves of α on the local skin friction coefficient in the y −direction for $Q = 0.1$. $A = 0.8$. $\phi = 0.1$. $\beta = 0.5$.

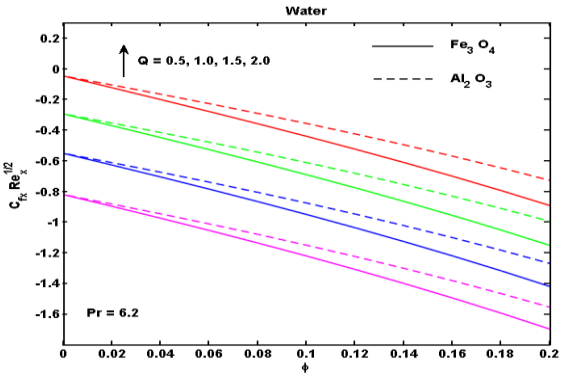

(a)

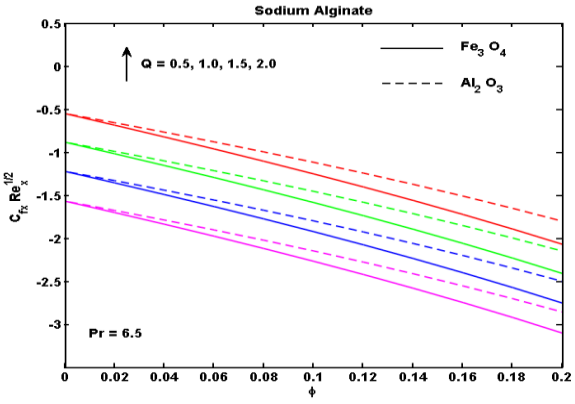

(b)

Figure 11. Curves of Q on the local skin friction coefficient in the $x-$direction for $A = 0.8$. $\alpha = 0.6$. $\phi = 0.1$. $\beta = 0.5$.

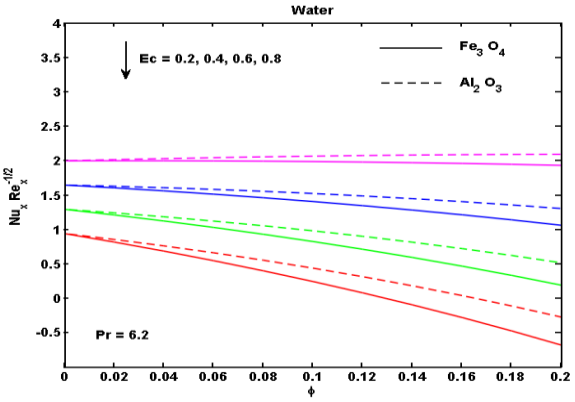

(a)

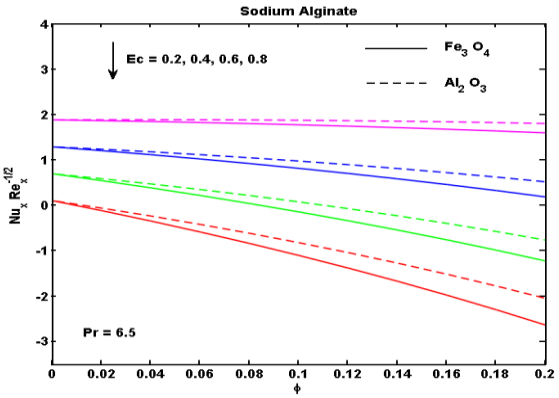

(b)

Figure 12. Curves of Ec on the local Nusselt number for $Q = 0.1$. $A = 0.8$. $\alpha = 0.6$. $\phi = 0.1$. $\beta = 0.5$.

Table 2. Nanofluid models [27].

Nano fluid properties	Applied model
Density	$\rho_{nf} = (1-\phi)\,\rho_f + \rho_s$
Thermal diffusivity	$\alpha_{nf} = \dfrac{k_{nf}}{(\rho\, C_p)_{nf}}$
Heat capacitance	$(\rho\, C_p)_{nf} = (1-\phi)\,(\rho\, C_p)_f + (\rho\, C_p)_s$
Kinematic viscosity	$\nu_{nf} = \dfrac{\mu_{nf}}{\rho_{nf}}$
Dynamic viscosity	$\mu_{nf} = \dfrac{\mu_f}{(1-\phi)^{2.5}}$
Thermal conductivity	$\dfrac{k_{nf}}{k_f} = \dfrac{k_s + 2k_f - 2\phi(k_f - k_s)}{k_s + 2k_f + \phi(k_f - k_s)}$

Conclusion

A thorough investigation is carried out for the viscous dissipating nanofluids of Fe_3O_4/Al_2O_3 nanoparticle within $H_2O/NaC_6H_9O_7$ base fluids on a Riga plate.

Specific non-dimensional regulating parameters affecting common profiles and the physical quantities are discussedand described in graphs and tables. The results are the following:

- Modified Hartmann number and stretching ratio parameter ameliorate the velocity profile.
- The presence of viscous dissipation benefits the temperature profile with the hiking Eckert number values.
- Velocity profile grows less due to increasing β.
- The modified Hartmann number organizes the numerical values of friction factor to become more intense.
- The development of Eckert number decreases the rate of heat transfer.

The most important conclusion is that, giving special importance to the relevant parameters make more clear that $H_2O - Al_2O_3$ nanofluid has high skin friction values and also that the rate of heat transfer is more desirable when compared with the other combination of nanofluids. Thus nanofluids with electromagnetohydrodynamics flow control, have very attractive features in material production, energy applications and even in medical engineering.

Table 3. $f''(0)$ and $g''(0)$ comparison for α with Wang [44], Hayat et al. [45] and Ganesh Kumar et al. [46]

	Wang [44]		Hayat et al. [45]		Ganesh Kumar et al. [46]		Present Result	
α	$-f''(0)$	$-g''(0)$	$-f''(0)$	$-g''(0)$	$-f''(0)$	$-g''(0)$	$-f''(0)$	$-g''(0)$
0	1	0	1	0	1	0	1.00000000	0
0.25	1.0488	0.1945	1.048810	0.19457	1.04906	0.19457	1.04881108	0.19456383
0.5	1.0930	0.4652	1.093095	0.465205	1.09324	0.46532	1.09309502	0.46520485
0.75	1.1344	0.7946	1.134500	0.794620	1.13458	0.79470	1.13448575	0.79461826
1	1.1737	1.1737	1.173721	1.173721	1.17378	1.17378	1.17372074	1.17372074

Table 4. Skin friction coefficient values for the base fluid H_2O with Fe_3O_4 and Al_2O_3.

Parameter	Value	$\frac{1}{(1-\phi)^{2.5}} f''(0)$		$\frac{1}{(1-\phi)^{2.5}} g''(0)$	
		Fe_3O_4	Al_2O_3	Fe_3O_4	Al_2O_3
A	0.5	-0.808079	-0.730127	-1.823157	-1.747242
	1.0	-1.016964	-0.943678	-1.781449	-1.705362
	1.5	-1.127532	-1.056401	-1.761324	-1.685311
α	0.5	-0.931467	-0.857656	-1.868107	-1.789211
	1.0	-1.023488	-0.945553	-1.636520	-1.566477
	1.5	-1.109072	-1.027305	-1.550743	-1.483965
ϕ	0.05	-0.745427	-0.707318	-1.556020	-1.517832
	0.10	-0.950529	-0.875863	-1.794484	-1.718410
	0.15	-1.173178	-1.061740	-2.056100	-1.940965
Q	0.5	1.220785	-1.150545	-1.763742	-1.687919
	1.0	-0.950529	-0.875863	-1.794484	-1.718410
	1.5	-0.691828	-0.612744	-1.821544	-1.745259

Table 5. Skin friction coefficient values for the base fluid $NaC_6H_9O_7$ with Fe_3O_4 and Al_2O_3

Parameter	Value	$\left(1+\frac{1}{\beta}\right)\alpha^{-3/2}\frac{1}{(1-\phi)^{2.5}} f''(0)$		$\left(1+\frac{1}{\beta}\right)\alpha^{-3/2}\frac{1}{(1-\phi)^{2.5}} g''(0)$	
		Fe_3O_4	Al_2O_3	Fe_3O_4	Al_2O_3
A	0.5	-1.692111	-1.562825	-3.104385	-2.971721
	1.0	-2.017838	-1.894969	-3.045223	-2.912761
	1.5	-2.167257	-2.047126	-3.024020	-2.891803
α	0.5	-1.884619	-1.761532	-3.179568	-3.042097
	1.0	-2.063767	-1.932976	-2.807299	-2.685188
	1.5	-2.228532	-2.090642	-2.669250	-2.552817
ϕ	0.05	-1.560767	-1.497460	-2.647837	-2.581239
	0.10	-1.921922	-1.797233	-3.061205	-2.928625
	0.15	-2.315287	-2.128370	-3.514706	-3.314165
Q	0.5	-2.265696	-2.145896	-3.029555	-2.897437
	1.0	-1.921922	-1.797233	-3.061205	-2.928625
	1.5	-1.584385	-1.454781	-3.091008	-2.958006
β	0.5	-1.921922	-1.797233	-3.061205	-2.928625
	1.0	-1.491598	-1.388277	-2.513521	-2.405211
	1.5	-1.328150	-1.233162	-2.300851	-2.201967

Table 6. Nusselt number values for $H_2O/NaC_6H_9O_7$base fluids with Fe_3O_4/Al_2O_3

Parameter	Value	Water		Sodium Alginate	
		Fe_3O_4	Al_2O_3	Fe_3O_4	Al_2O_3
A	0.5	1.378464	1.509588	0.666796	0.850717
	1.0	0.987730	1.125889	0.193559	0.386154
	1.5	0.780329	0.921751	-0.006512	0.189267
α	0.5	1.242244	1.366485	0.535187	0.708499
	1.0	0.097071	0.304758	-1.205483	-0.910961
	1.5	-2.502846	-2.140483	-5.020896	-4.498302
ϕ	0.05	1.306378	1.373382	0.680881	0.774608
	0.10	1.114704	1.250758	0.330488	0.520755
	0.15	0.889489	1.097296	-0.068841	0.221838
Q	0.5	0.789859	0.932996	0.013473	0.210464
	1.0	1.114704	1.250758	0.330488	0.520755
	1.5	1.354690	1.481538	0.595430	0.777505
Ec	0.2	1.984290	2.062807	1.767137	1.866779
	0.4	1.404566	1.521441	0.809371	0.969429
	0.6	0.824842	0.980075	-0.148394	0.072080
β	0.5	-	-	0.3304488	0.520755
	1.0	-	-	0.652068	0.823263
	1.5	-	-	0.786286	0.949429

Nomenclature

A	Material Constant
$a\,.\,b$	Constants
a_1	The width of the magnets between the electrodes
C_p	Specific heat coefficient $[J.kg.K]$
$C_{fx}\,.\,C_{fy}$	Skin friction coefficients
Ec	Eckert number
$f.g$	Dimensionless stream functions
j_0	Applied current density in electrodes
k	Thermal conductivity
M_0	Magnetization of the permanent magnets
Nu_x	Local Nusselt number
Pr	Prandtl number
Q	Modified Hartmann number
q_w	Wall heat flux $[W/m^2]$
$\mathrm{Re}_x\,.\,\mathrm{Re}_y$	Local Reynolds number
T	Local fluid temperature $[K]$
T_w	Temperature at the surface of the plate $[K]$
T_∞	Free stream temperature $[K]$
$U_w\,.\,V_w$	Stretching velocities
$u.v.w$	Components of velocity $[m/s]$
$x.y.z$	Coordinates $[m]$

Greek Letters

α	Stretching ratio parameter
α_{nf}	Thermal diffusivity of the nanofluid $[m^2/s]$
β	Casson parameter
ϕ	Volume fraction of nanoparticle
η	Similarity variable
μ	Absolute viscosity $[Ns/m^2]$
ν	Kinematic viscosity $[m^2/s]$
ρ	Density $[kg/m^3]$
θ	Dimensionless temperature
ψ	Stream function
τ_w	Viscous stress at the surface of the plate $[Nm^{-2}]$

Subscripts

nf	Nanofluid
f	Base fluid
s	Solid nanoparticles
∞	Boundary layer edge

References

[1] Turkyilmazoglu, M., 2020. Single phase nanofluids in fluid mechanics and their hydrodynamic linear stability analysis. *Computer methods and programs in biomedicine*, *187*, p.105171.

[2] Ahmad, R., Mustafa, M. and Turkyilmazoglu, M., 2017. Buoyancy effects on nanofluid flow past a convectively heated vertical Riga-plate: A numerical study. *International Journal of Heat and Mass Transfer*, *111*, pp.827-835.

[3] Gholinia, M., Kiaeian Moosavi, S.A.H., Gholinia, S. and Ganji, D.D., 2019. Numerical simulation of nanoparticle shape and thermal ray on a $CuO/C_2H_6O_2–H_2O$ hybrid base nanofluid inside a porous enclosure using Darcy's law. *Heat Transfer—Asian Research*, *48*(7), pp.3278-3294.

[4] Turkyilmazoglu, M., 2019. Fully developed slip flow in a concentric annuli via single and dual phase nanofluids models. *Computer methods and programs in biomedicine*, *179*, p.104997.

[5] Gholinia, M., Pourfallah, M. and Chamani, H.R., 2018. Numerical investigation of heat transfers in the water jacket of heavy duty diesel engine by considering boiling phenomenon. *Case studies in thermal engineering*, *12*, pp.497-509.

[6] Ghadikolaei, S.S. and Gholinia, M., 2020. 3D mixed convection MHD flow of GO-MoS_2 hybrid nanoparticles in $H_2O–(CH_2OH)_2$ hybrid base fluid under the effect of H_2 bond. *International Communications in Heat and Mass Transfer*, *110*, p.104371.

[7] Dibaei, M. and Kargarsharifabad, H., 2017. New achievements in Fe_3O_4 nanofluid fully developed forced convection heat transfer under the effect of a magnetic field: An experimental study. *Journal of Heat and Mass Transfer Research*, *4*(1), pp.1-11.

[8] Tajik, M., Dehghan, M. and Zamzamian, A., 2015. Analysis of variance of nanofluid heat transfer data for forced convection in horizontal spirally coiled tubes. *Journal of Heat and Mass Transfer Research*, *2*(2), pp.45-50.

[9] Gholinia, M., Moosavi, S.K., Pourfallah, M., Gholinia, S. and Ganji, D.D., 2019. A numerical treatment of the $TiO2/C_2H_6O_2–H_2O$ hybrid base nanofluid inside a porous cavity under the impact of shape factor in MHD flow. *International Journal of Ambient Energy*, pp.1-8. (Doi: 10.1080/01430750.2019.1614996).

[10] Gailitis, A., 1961. On the possibility to reduce the hydrodynamic drag of a plate in an electrolyte. *Appl. Magnetohydrodynamics, Rep. Inst. Phys. Riga*, *13*, pp.143-146.

[11] Hakeem, A.K., Nayak, M.K. and Makinde, O.D., 2019. Effect of exponentially variable viscosity and permeability on Blasius flow of Carreau nano fluid over an electromagnetic plate through a porous medium. *Journal of Applied and Computational Mechanics*, *5*(2), pp.390-401.

[12] Ragupathi, P., Hakeem, A.A., Saranya, S. and Ganga, B., 2019. Non-Darcian three-dimensional flow of Fe_3O_4/Al_2O_3 nanoparticles with $H_2O/NaC_6H_9O_7$ base fluids past a Riga plate embedded in a porous medium. *The European Physical Journal Special Topics*, *228*(12), pp.2571-2600.

[13] Ragupathi, P., Hakeem, A.A., Al-Mdallal, Q.M., Ganga, B. and Saranya, S., 2019. Non-uniform heat source/sink effects on the three-dimensional flow of Fe_3O_4/Al_2O_3 nanoparticles with different base fluids past a Riga plate. *Case Studies in Thermal Engineering*, *15*, p.100521.

[14] Abdul Hakeem, A.K., Ragupathi, P., Saranya, S. and Ganga, B., 2020. Three dimensional non-linear radiative nanofluid flow over a Riga plate. *Journal of Applied and Computational Mechanics*, *6*(4), pp.1012-1029.

[15] Nasir, N.A.A.M., Ishak, A. and Pop, I., 2019. Stagnation point flow and heat transfer past a permeable stretching/shrinking Riga plate with velocity slip and radiation effects. *Journal of Zhejiang University-SCIENCE A*, *20*(4), pp.290-299.

[16] Shafiq, A., Hammouch, Z. and Turab, A., 2018. Impact of radiation in a stagnation point flow of Walters' B fluid towards a Riga plate. *Thermal Science and Engineering Progress*, *6*, pp.27-33.

[17] Zaib, A., Haq, R.U., Chamkha, A.J. and Rashidi, M.M., 2019. Impact of partial slip on mixed convective flow towards a Riga plate comprising micropolar TiO_2-kerosene/water nanoparticles. *International Journal of Numerical Methods for Heat & Fluid Flow*, 29(5), pp.1647-1662.

[18] Abbas, T., Bhatti, M.M. and Ayub, M., 2018. Aiding and opposing of mixed convection Casson nanofluid flow with chemical reactions through a porous Riga plate. *Proceedings of the institution of mechanical engineers, part E: journal of process mechanical engineering*, *232*(5), pp.519-527.

[19] Iqbal, Z., Azhar, E., Mehmood, Z. and Maraj, E.N., 2018. Unique outcomes of internal heat generation and thermal deposition on viscous dissipative transport of viscoplastic fluid over a Riga-plate. *Communications in Theoretical Physics*, *69*(1), p.68-76.

[20] Nayak, M.K., Shaw, S., Makinde, O.D. and Chamkha, A.J., 2018. Effects of homogenous–heterogeneous reactions on radiative NaCl-CNP nanofluid flow past a convectively heated vertical Riga plate. *Journal of Nanofluids*, *7*(4), pp.657-667.

[21] Anjum, A., Mir, N.A., Farooq, M., Khan, M.I. and Hayat, T., 2018. Influence of thermal stratification and slip conditions on stagnation point flow towards variable thicked Riga plate. *Results in Physics*, *9*, pp.1021-1030.

[22] Shaw, S., Nayak, M.K. and Makinde, O.D., 2018. Transient rotational flow of radiative nanofluids over an impermeable Riga plate with variable properties, *Defect and Diffusion Forum*, 387, pp. 640-652.

[23] Hussain, A., Akbar, S., Sarwar, L., Nadeem, S. and Iqbal, Z., 2019. Effect of time dependent viscosity and radiation efficacy on a non-Newtonian fluid flow. *Heliyon*, *5*(2), p.e01203.

[24] Hakeem, A.A., Saranya, S. and Ganga, B., 2017. Comparative study on Newtonian/non-Newtonian base fluids with magnetic/non-magnetic nanoparticles over a flat plate with uniform heat flux. *Journal of Molecular Liquids*, *230*, pp.445-452.

[25] Rundora, L. and Makinde, O.D., 2018. Unsteady mhd flow of non-newtonian fluid in a channel filled with a saturated porous medium with asymmetric navier slip and convective heating, Applied Mathematics & Information Sciences, 12(3), 483-493, (2018).

[26] Bayareh, M. and Afshar, N., 2020. Forced convective heat transfer of non-Newtonian CMC-based CuO nanofluid in a tube. *Journal of Heat and Mass Transfer Research*, *7*(2), pp.155-163.

[27] Saranya, S., Ragupathi, P., Ganga, B., Sharma, R.P. and Hakeem, A.A., 2018. Non-linear radiation effects on magnetic/non-magnetic nanoparticles with different base fluids over a flat plate. *Advanced Powder Technology*, *29*(9), pp.1977-1990.

[28] Eid, M.R. and Mahny, K.L., 2017. Unsteady MHD heat and mass transfer of a non-Newtonian nanofluid flow of a two-phase model over a permeable stretching wall with heat generation/absorption. *Advanced Powder Technology*, *28*(11), pp.3063-3073.

[29] Durgaprasad, P., Varma, S.V.K., Hoque, M.M. and Raju, C.S.K., 2019. Combined effects of Brownian motion and thermophoresis parameters on three-dimensional (3D) Casson nanofluid flow across the porous layers slendering sheet in a suspension of graphene nanoparticles. *Neural Computing and Applications*, *31*(10), pp.6275-6286.

[30] Raju, C.S., Sandeep, N., Ali, M.E. and Nuhait, A.O., 2019. Heat and mass transfer in 3-D MHD Williamson-Casson fluids flow over a stretching surface with non-uniform heat source/sink. *Thermal Science*, *23*(1), pp.281-293.

[31] Zia, Q.Z., Ullah, I., Waqas, M., Alsaedi, A. and Hayat, T., 2018. Cross diffusion and exponential space dependent heat source impacts in radiated three-dimensional (3D) flow of Casson fluid by heated surface. *Results in physics*, *8*, pp.1275-1282.

[32] Prashu and Nandkeolyar, R., 2018. A numerical treatment of unsteady three-dimensional hydromagnetic flow of a Casson fluid with Hall and radiation effects. *Results in Physics*, *11*, pp.966-974.

[33] Muhammad, T., Hayat, T., Shehzad, S.A. and Alsaedi, A., 2018. Viscous dissipation and Joule heating effects in MHD 3D flow with heat and mass fluxes. *Results in physics*, *8*, pp.365-371.

[34] Kumar, K.G., Ramesh, G.K., Gireesha, B.J. and Gorla, R.S.R., 2018. Characteristics of Joule heating and viscous dissipation on three-dimensional flow of Oldroyd B nanofluid with thermal radiation. *Alexandria Engineering Journal*, *57*(3), pp.2139-2149.

[35] Saleem, S., Nadeem, S., Rashidi, M.M. and Raju, C.S.K., 2019. An optimal analysis of radiated nanomaterial flow with viscous dissipation and heat source. *Microsystem Technologies*, *25*(2), pp.683-689.

[36] Nayak, M.K., Shaw, S., Makinde, O.D. and Chamkha, A.J., 2019. Investigation of partial slip and viscous dissipation effects on the radiative tangent hyperbolic nanofluid flow past a vertical permeable Riga plate with internal heating: Bungiorno model. *Journal of Nanofluids*, *8*(1), pp.51-62.

[37] Mahanthesh, B. and Gireesha, B.J., 2018. Scrutinization of thermal radiation, viscous dissipation and Joule heating effects on Marangoni convective two-phase flow of Casson fluid with fluid-particle suspension. *Results in physics*, *8*, pp.869-878.

[38] Upreti, H., Pandey, A.K. and Kumar, M., 2018. MHD flow of Ag-water nanofluid over a flat porous plate with viscous-Ohmic dissipation, suction/injection and heat generation/absorption. *Alexandria engineering journal*, *57*(3), pp.1839-1847.

[39] Hussanan, A., Salleh, M.Z., Khan, I. and Shafie, S., 2018. Analytical solution for suction and injection flow of a viscoplastic Casson fluid past a stretching surface in the presence of viscous dissipation. *Neural computing and applications*, *29*(12), pp.1507-1515.

[40] Ramandevi, B., Reddy, J.R., Sugunamma, V. and Sandeep, N., 2018. Combined influence of viscous dissipation and non-uniform heat source/sink on MHD non-Newtonian fluid flow with Cattaneo-Christov heat flux. *Alexandria Engineering Journal*, *57*(2), pp.1009-1018.

[41] Ghaffarpasand, O., 2018. Characterization of unsteady double-diffusive mixed convection flow with soret and dufour effects in a square enclosure with top moving lid. *Journal of Heat and Mass Transfer Research*, *5*(1), pp.51-68.

[42] Hassanzadeh, R. and Nasrollahzadeh, S., 2020. Heat transfer enhancement in a spiral plate heat exchanger model using continuous rods. *Journal of Heat and Mass Transfer Research*, *7*(1), pp.39-53.

[43] Noghrehabadi, A., Hajidavalloo, E. and Moravej, M., 2016. An experimental investigation of performance of a 3-D solar conical collector at different flow rates. *Journal of Heat and Mass Transfer Research*, *3*(1), pp.57-66.

[44] Wang, C.Y., 1984. The three-dimensional flow due to a stretching flat surface. *The physics of fluids*, *27*(8), pp.1915-1917.

[45] Hayat, T., Shehzad, S.A. and Alsaedi, A., 2013. Three-dimensional stretched flow of Jeffrey fluid with variable thermal conductivity and thermal radiation. *Applied Mathematics and Mechanics*, *34*(7), pp.823-832.

[46] Kumar, K.G., Rudraswamy, N.G. and Gireesha, B.J., 2017. Effects of mass transfer on MHD three dimensional flow of a Prandtl liquid over a flat plate in the presence of chemical reaction. *Results in Physics*, *7*, pp.3465-3471.